Article

Experimental and Theoretical Investigation of High-Resolution X-ray Absorption Spectroscopy (HR-XAS) at the Cu *K*-Edge for Cu$_2$ZnSnSe$_4$

Wei Xu [1,2,*] , Yujun Zhang [1] , Kenji Ishii [3] , Hiroki Wadati [4] , Yingcai Zhu [5] , Zhiying Guo [1] , Qianshun Diao [1] , Zhen Hong [1] , Haijiao Han [1] and Lidong Zhao [5]

1   Beijing Synchrotron Radiation Facility, Institute of High Energy Physics, Chinese Academy of Sciences, Beijing 100049, China
2   International Centre for Material Science Superstripes, RICMASS, Via dei Sabelli 119A, 00185 Rome, Italy
3   Synchrotron Radiation Research Center, National Institutes for Quantum Science and Technology, Sayo-gun, Hyogo 679-5148, Japan
4   Graduate School of Materials Science, University of Hyogo, 3-2-1 Kouto, Kamigori-cho, Ako-gun, Hyogo 678-1297, Japan
5   School of Materials Science and Engineering, Beihang University, Beijing 100191, China
*   Correspondence: xuw@ihep.ac.cn

Abstract: Energy sustainability is critical for social activities in the human world. The quaternary compound Cu$_2$ZnSnSe$_4$ (CZTSe), as a promising candidate for thin-film solar cell absorption with medium-level thermoelectric performance, is of interest for the purpose of utilizing solar energy. The defect chemistry and atomic ordering in this particular compound also triggers interests in understanding its crystallographic structure as well as defects. Hereby, high energy resolution X-ray absorption spectroscopy is employed to investigate the electronic and geometric structural complexity in pristine and cobalt-doped Cu$_2$ZnSnSe$_4$. The occupational atomic sites of Cu are found to be mixed with the Zn atoms, forming Cu$_{Zn}$ anti-defects, which serve as a knob to tune local electronic structures. With proper doping, the band structure can be manipulated to improve the optical and thermoelectric properties of the CZTSe compounds.

Keywords: Cu$_2$ZnSnSe$_4$; solar cell; X-ray absorption spectroscopy (XAS)

1. Introduction

Solar energy is critical for human activities and represents one of the sustainable energy resources that promise to provide clean energy. Full exploitation of solar energy, however, still remains a huge challenge, though solar energy technology has been developed over decades. Photovoltaics, fabricated with cadmium telluride (CdTe) and copper indium gallium selenide (CIGS) sandwiched between cover and metal electrodes, represent a great potential source for solar energy harvesting [1]. Research in this field has exploded over the past two decades, with cell efficiency boosted to a record high of 50%. The rising efficiency of the solar cell relies on breakthroughs in materials sciences and technological innovations in hierarchical structures. All of these are based on deep understanding of materials structures, from meso to atomic scales. Quaternary compound Cu$_2$ZnSnSe$_4$ (CZTSe), consisting of low-cost and abundant chemical elements, is one of the candidates for a next-generation solar cell absorber due to its strong optical direct band gap ~1.5 eV, within the range of optimal optical absorption on the solar spectrum (~1.0–1.7 eV) [2]. On the other hand, thanks to its intrinsic low thermal conductivity, CZTSe-based compounds have been also explored as candidates for thermoelectric materials with a medium level thermoelectric performance [3,4]. The low thermal conductivity correlates with its relatively low vibrational energy [5]. A recent study also unveiled the rich defect chemistry in CZTSe-based quaternary compounds [6]. Based on first-principles calculations, Chen et al. [7,8],

revealed that there exists a large variety of intrinsic defects which impose important influence on optical and electrical properties, such as anti-site defects. An anti-site defect is the occupation of alien atoms on the ideal atomic site, allocated to specific elements. Of particular interest, the band gap energy varies with respect to the type of anti-site defects. This also highlights that the complexity of the atomic and electronic structure of CZTSe.

There are two main tetragonal structural types for CZTSe: the kesterite type and the stannite type [9]. The debate over structural origins and intrinsic point defects has captured much interests over past years. A neutron diffraction study [10] by S. Schorr indicated that CZTSe can only form a kesterite type instead of stannite type. A high-resolution neutron powder diffraction experiment with full Rietveld refinement performed on the sister compound Cu_2ZnSnS_4 (CZTS) indicated that the phase structure is a kesterite type with significant cation disorder [11]. Another important technique to address this structural complexity is the anomalous X-ray diffraction or resonant X-ray diffraction [12–15] to be performed near the absorption edge of selected elements. Because the scattering power of the resonant atoms can be reduced at the energy near their absorption edge, it is then possible to provide an element-specific contrast, in this case, of Cu and Zn. Previously, we have performed an atomic dynamics study using temperature-dependent extended X-ray absorption fine structure (EXAFS) [5]. Nevertheless, the near-edge region of the X-ray absorption spectroscopy is complicated and some of the spectral features were not clearly shown due to the relatively poor energy resolution for conventional X-ray absorption spectroscopy (XAS) setup.

In this contribution, we focus on the electronic structure as well as structural complexity of CZTSe using high energy resolution X-ray absorption spectroscopy (HR-XAS). The incident energy bandwidth of HR-XAS (~0.3 eV) is reduced drastically with respect to conventional XAS (~1.8 eV). In this way, only core-hole lifetime effects dominate the spectral broadening, which is also contributed to by the instrumental function in conventional XAS [16]. Combining the improved energy resolution of the experimental setup and theoretical simulations could provide a profound understanding of the local electronic structures in CZTSe.

2. Results

The structural differences of the two proposed tetragonal structures of CZTSe are depicted in Figure 1. The atomic sites are listed in Table 1 for comparison. The two types of crystal structure have different symmetry, and the kesterite has lower symmetry than stannite. The atomic occupation of Cu and Zn atoms dictates the crystal structure. As highlighted in the shadow plane, Cu and Zn atoms appear within the same plane for kesterite structures, but merely Cu atoms exist in the plane for stannite structures. Additionally, a proposed disordered kesterite structure refers to a structure with fractional Cu/Zn occupation [12]. The assignment of the atomic sites is the same for Sn and Se atoms in the two structures. On the other hand, the Cu and Zn occupation sites are different between the two structures. In a kesterite structure, Cu occupies two atomic sites, namely the 2a (0,0,0) site and 2d (0,1/2,3/4) site, while Zn occupies the 2c (0,1/2,1/4) site. In a stannite structure, Cu and Zn occupy 4d (0,1/2,1/4) and 2a (0,0,0) site, respectively. Nevertheless, the site symmetry of Cu in kesterite is identical to that in stannite. The site symmetry of Zn is similar to that of Cu in kesterite; while the site symmetry of Zn is different from that of Cu in stannite. The electronic structure calculations [17–20] indicated that the kesterite structure can be classified as a topological insulator (https://www.topologicalquantumchemistry.org/#/detail/189278 accessed on 11 January 2022) while the stannite structure can be classified as a trivial metal or insulator (https://www.topologicalquantumchemistry.org/#/detail/184474 accessed on 11 January 2022). This classification highlights the link between the band topology and local chemical bonding.
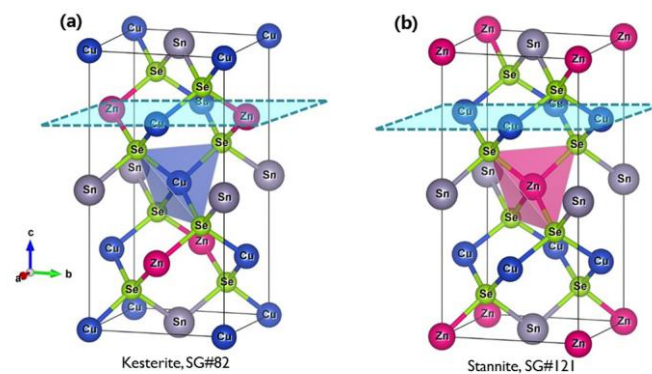
Figure 1. Two tetragonal-type crystal structures of the $Cu_2ZnSnSe_4$: (**a**) kesterite and (**b**) stannite. A shadow plane is to highlight the occupation of Cu/Zn.

Table 1. Comparison of the space group and atomic occupation as well as the site symmetry of the two tetragonal types of crystal structure.

Crystal	Kesterite		Stannite	
Space group	$I\bar{4}$ (#82)	Site symmetry	$I\bar{4}2$ m (#121)	Site symmetry
Zn	2c (0,1/2,1/4)	−4..	2a (0,0,0)	−42 m
Cu	2a (0,0,0)	−4..	4d (0,1/2,1/4)	−4..
	2d (0,1/2,3/4)	−4..		
Sn	2b (0,0,1/2)	−4..	2b (0,0,1/2)	−42 m
Se	8g (x,y,z)	1	8i (x,x,z)	..m

To further prompt the understanding of the local structural distortion as well as its influences on local orbitals, experimental and theoretical simulation of high-resolution XAS were performed.

2.1. High Energy Resolution XAS vs. Conventional XAS

2.1.1. Temperature Effects

Lowering sample temperature is an effective way to reduce the thermally induced disordering of atomic bonds. The detailed temperature-induced vibrational effects were previously studied using the temperature-dependent EXAFS technique [5], revealing the low Einstein temperature (~250 K at the Cu K-edge) of this compound. In Figure 2, we compared the conventional XAS results at the Cu *K*-edge for CZTSe and co-doped CZTSe measured at 10 K and room temperature to highlight the temperature-induced effects. There is a pronounced 1s–4p transition denoted as feature A at 8985 eV and a flat feature denoted as B at 8990 eV in the white-line region which mainly reflects the unoccupied 4p electronic density of states of the excited Cu absorber. The feature C at 8995 eV also originates from the 1s–4p transition. Unlike the other two features, a significant temperature effect is manifested by the feature C at 8995 eV which becomes sharper at 10 K than at room temperature. At low temperature, the atoms are tranquilized, and thermally activated disordering is reduced significantly. Consequently, the spectra at 10 K become less broadened with respect to the spectrum at room temperature. The trend is similar for both pristine and doped species. Therefore, feature C is also contributed by the multiple scattering of the local coordinate atoms. Hence, the spectral contrast can be enhanced by cooling the samples. On the other hand, to perform HR-XAS at a beamline with high brilliance source, the radiation damage (heating effects) could be effectively avoided by cooling the sample. Hence, the HR-XAS experiment were performed only at 10 K.
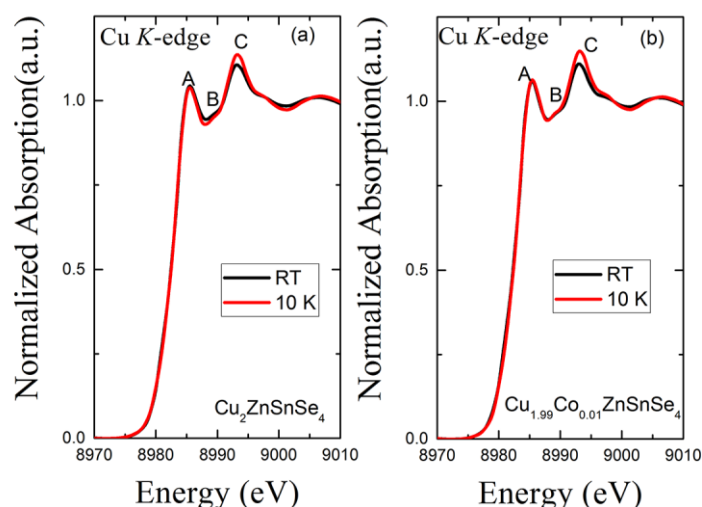
Figure 2. Comparison of conventional XAS results at the Cu *K*-edge for (**a**) pristine and (**b**) co-doped CZTSe at room temperature and 10K, respectively. Spectral features A, B, C are denoted. See the main text for assignment.

2.1.2. Doping Effects

Doping is an effective strategy to tune the chemical potential and concentration charge-carrier in thermoelectrics. With Co^{2+} replacing Cu^{1+}, it was found that the electrical conductivity and Seebeck coefficient can be tuned slightly [5]. Herein, we compare dilute doped species to see if doping effects can be manifested in HR-XAS.

To further examine the doping effects at 10K, we compared the Cu *K*-edge XAS and high-resolution XAS results in Figure 3. In this way, the temperature induced disordering effects are minimized and spectral difference becomes discernible. For conventional XAS, the peak intensity is slightly higher in doped CZTSe with respect to the pristine CZTSe while the spectral shape remains identical, giving little information. With the improved energy resolution, the high-resolution XAS sharpens the spectral features, in particular, the feature B, at around 8990 eV in between feature A and C. There exist three pronounced spectral features in the HR-XAS spectra for both pristine and doped species. To further understand the details of the HR-XAS spectra, theoretical simulations of the spectra are necessary.
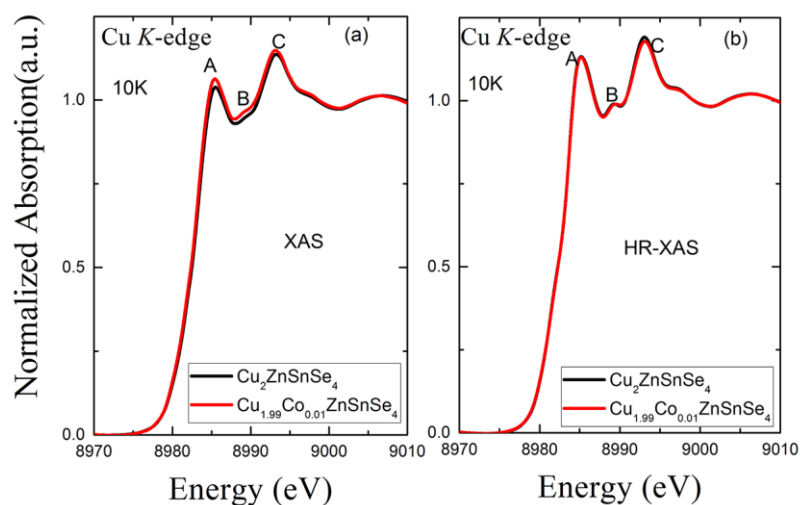

Figure 3. Comparison of (**a**) conventional XAS and (**b**) high-resolution XAS (HR-XAS) spectra at the Cu *K*-edge for pristine and co-doped CZTSe at 10 K. Spectral features A, B, C are denoted. See the main text for assignment.

2.1.3. Stannite (SG121) vs. Kesterite (SG82) Phase from Theoretical Simulated Spectra

Hence, we performed simulation of the XAS at the Cu *K*-edge for two Cu sites in kesterite CZTSe (SG82) versus one Cu site in stannite CZTSe (SG121), based on the crystallographic structure. As shown in Figure 4, There are three pronounced peaks in the near-edge region for all Cu sites in either the kesterite or stannite structure. As aforementioned, the site symmetry of Wyckoff sites Cu 2a and Cu 2d are identical while the spectral differences are significant in the first peak. The spectrum of Cu 2d site exhibits a stronger intensity with a peak at 8985 eV reflecting more empty states in this region than the Cu 2a in kesterite and the Cu 4d sites in the stannite structure, respectively. The atomic coordinate of the Cu 2d site is 2d (0,1/2,3/4); while the atomic coordinate of Cu 2a and Cu 4d sites in the kesterite structure are swapped with Zn 2a and Zn 2c site in the stannite structure.
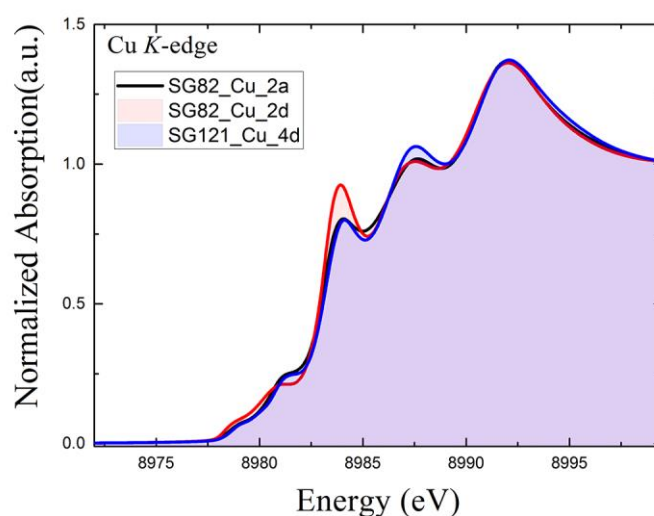

Figure 4. Comparison of theoretically simulated XAS at the Cu *K*-edge for two atomic sites in kesterite structure and one site in stannite structure.

In Figure 5, comparison is focused on the projected density of states on each electronic orbital of Cu to understand its electronic structure. Theoretically, there are four features noted as a, b, c and d in the near-edge region. The assignment of the features to the orbitals are as follows: (1) feature a is contributed by the hybridization of s and d; (2) the features b, c and d resemble the p states, reflecting the 1s-4p transition. The m quantum number-induced splitting of the p orbitals exhibits anisotropic behavior, i.e., the p_z component shows stronger contributions to the features b and d, while the p_x/p_y components contribute much to the feature c, as well as feature b and d. In other words, the feature b in Figure 5 corresponds to the first observable feature A in the experimental spectra in Figure 3. The intensity of this feature is related to the directionality of the p orbitals. Additionally, if we take a closer look, the intensity ratio of the peaks in experimental spectra is more similar to the p_z density of states of Cu atoms.

In order to further distinguish the atomic site contribution, we compare the projected density of states for each atom in the CZTSe. In Figure 6, the excited Cu partial density of states (PDOS) exhibit three features, with intensity increasing from low to higher energy. Interestingly, the PDOS of Zn also exhibit three features in the region overlapped with that of Cu. However, the PDOS of Zn exhibit the strongest intensity in the peak ~4 eV above the Fermi energy, then become weaker in the higher energy region.
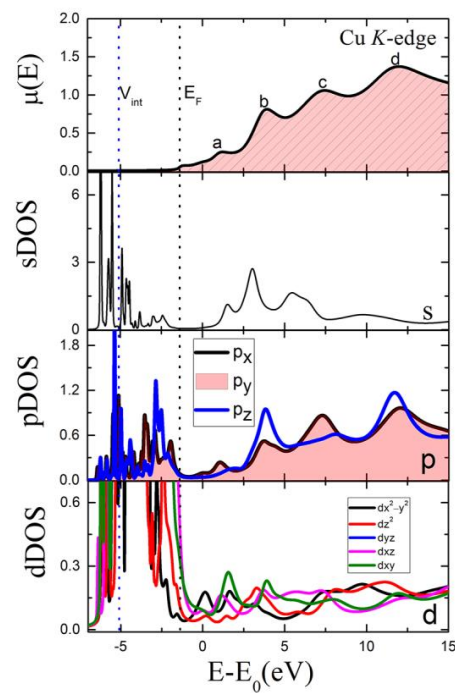
Figure 5. Comparison of the simulated spectra with respect to the partial density of states projected on s, p and d split orbitals of Cu elements. V_{int} refers to the constant energy for imposing a muffin-tin scheme and E_F is the Fermi energy. Spectral features a, b, c, d are denoted. See the main text for assignment. Note that py is overlapped with px in pDOS while dyz is overlapped with dxz in dDOS, indicating that the system is isotropic along xy plane.
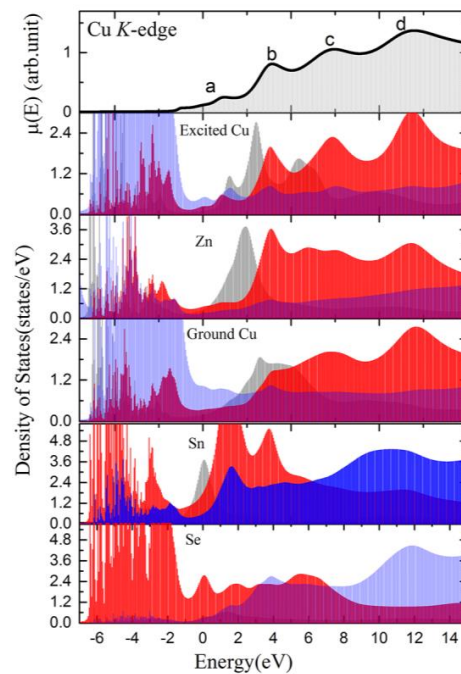

Figure 6. Comparison of the element specific partial density of states projected on different atoms in CZTSe. s, p and d orbitals are black, red and blue shadowed, respectively. The "Excited Cu" and "Ground Cu" refer to the central Cu absorber and spectator Cu atoms, respectively. The Cu-p (red), Zn-p (red), Sn-d (blue), Se-p (red) orbitals are emphasized while the rest orbitals are plotted in transparent mode. Spectral features a, b, c, d are denoted as the same notation with Figure 5.

Taking into account the possible anti-site defects [8] with occupation of Cu at other atomic sites, we simulated the spectra with different occupation sites. As shown in Figure 7, the spectra of Cu at Zn exhibit the strongest peaks at a low energy region, in contrast with the ideal Cu site. This is in good agreement with the partial density of states calculation shown in Figure 6. For Cu at the Sn site, there are also three peaks in the spectrum but the peak position shifted with respect to original spectrum due to the different atomic bond, but similar tetrahedral coordination, consisting of four Se atoms. The Cu at the Se site mode gives rise to a totally different spectrum.
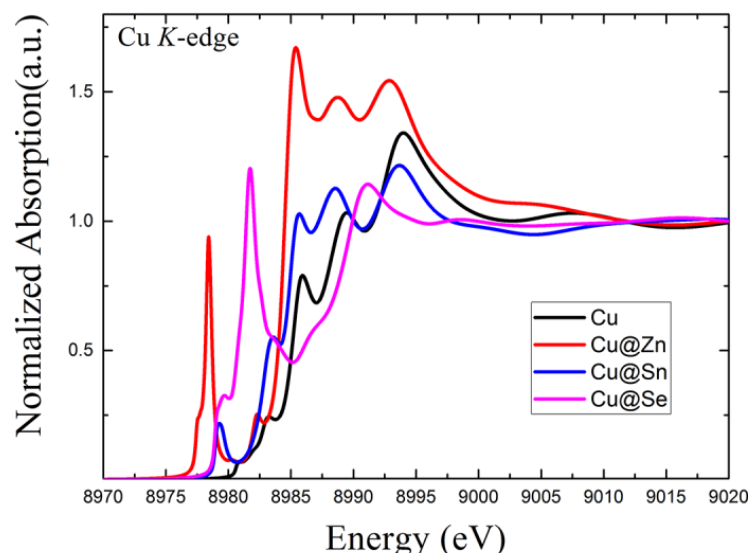

Figure 7. Simulated spectra with Cu occupying different atomic sites in CZTSe.

3. Discussion

Based on the experimental spectra and theoretical simulations shown in the Results section, we can attempt to decode the structural complexity of CZTSe. The high resolution XAS results confirm the three distinguishable peaks in both pristine and doped CZTSe. The intensity of peak A at 8985 eV is slightly weaker than that of peak C at 8993 eV, while the intensity of peak B at 8989 eV is much lower than that of peak A and peak C (Figure 3b). Nevertheless, the intensity ratio in the experimental Cu *K*-edge spectra cannot be reproduced by simply employing the crystallographic structure either from the kesterite or stannite structural type (Figure 4), though the theoretical simulation methods [21] are well established in many applications.

Hence, we must wonder whether there exists local structural disordering. Local structural disorder is not discernible by diffraction technique, which is merely sensitive to long-range ordering (LRO) [22]. It has been recognized that the Cu/Zn anti-site defects are ubiquitous in CZTSe [23,24]. Considering the substitution calculations in Figure 7, the highest peak lies in the high energy region at 8983 eV in the original model, while shifts to low energy region at 8985 eV in a model with Cu occupying the Zn site. Consequently, it is consistent to conclude that both Cu and Zn sites are occupied by the Cu atoms in CZTSe with certain ratio. It is unlikely that Cu would occupy the Se site and the probability for Cu to occupy Sn site is also low.

Based on the calculations of different atomic sites (Figure 4) and the density of states projected at different orbitals (Figure 5) as well as the density of states projected at different atoms (Figure 6), it is observed that: (1) the peak at 8985 eV is more intense for the Cu occupied 2d (0,1/2,3/4) atomic site in a kesterite structure; (2) peaks at 8985 eV and 8993 eV are more intense and the peak at 8990 eV is much weaker if the p_z orbital of Cu dominates; (3) peaks at 8990 eV and 8993eV are more intense if the p_x orbital of Cu dominates; (4) the occupation of Cu at Zn site will gives rise more empty states with low energy near Fermi

energy, giving rise to a strong peak at 8985 eV. Upon doping, certain number of Cu^{1+} are replaced by Co^{2+}. It is suspected that the occupation of Zn at Cu would be suppressed. Nevertheless, the HR-XAS spectra, as an average probe, measures all Cu atoms, and the local coordination environment for the majority of Cu atoms is identical for pristine and doped species.

4. Materials and Methods

Polycrystalline $Cu_2ZnSnSe_4$ and $Cu_{1.99}Co_{0.01}ZnSnSe_4$ were synthesized using ball-milling and sintered by spark plasma sintering (SPS) based on the method as described previously [5]. Pellets of about $10 \times 10 \times 2$ mm^3 were cut from the ingot for XAS measurements. The low-temperature high-resolution XAS (HR-XAS) were performed at the RIXS end-station of BL11XU in SPring-8. The samples were mounted on a He closed-cycle cryostat and cooled down to 10 K. The incident beam was first monochromatized by a Si(111) double crystal monochromator, followed by a Si(400) channel-cut monochromator. A PIN photodiode was used to detect the total fluorescence yield. The incident bandwidth is estimated to be less than 0.3 eV at the Cu *K*-edge. Owing to the instrument limitation, the HR-XAS is limited in the collecting energy range, but does allow the collection of spectra with sharp spectral features in the near-edge region. Conventional Cu *K*-edge XAS was performed at the 1W1B beamline of Beijing Synchrotron Radiation Facility, in transmission mode, using a Si(111) double crystal monochromator which provides an incident bandwidth of about 1.8 eV at the Cu *K*-edge [5]. The low temperature measurements were performed for samples mounted in a continuous flow He cryostat. The theoretical simulations of the spectra were performed using FDMNES code [25]. The simulations were performed using the full multiple scattering theory based on the muffin-tin (MT) approximation for the potential shape of the atomic potential. The MT radii were adjusted to create a good overlap between the different spherical potentials. A relativistic spin−orbit calculation was performed. In the calculation, the Hedin−Lundqvist exchange potential was applied. To account for improved energy resolution, the experimental broadening parameter in the calculations is not considered anymore.

5. Conclusions

The electronic structure in the unoccupied states and local structural ordering in solar cell/thermoelectric material, $Cu_2ZnSnSe_4$, has been studied using HR-XAS and theoretical calculations. Through detailed calculations and sharpened spectral features from HR-XAS, it is summarized that the local structure coordination environment of Cu in CZTSe is disordered; this is induced by the mixed occupation of Cu atoms at Zn sites, and vice versa. It is suspected that the subtle changes in the electronic state may have an impact on the electronic and optical properties of CZTSe.

Author Contributions: Conceptualization, W.X.; methodology, W.X., Y.Z. (Yujun Zhang), K.I., H.W.; formal analysis, W.X., Y.Z. (Yujun Zhang), K.I., H.W., Y.Z., Z.G., Q.D., Z.H. and H.H.; investigation, W.X., Y.Z. (Yujun Zhang), K.I., H.W., Y.Z. (Yingcai Zhu), L.Z., Z.G.; data curation, W.X., Y.Z. (Yujun Zhang), K.I. and H.W.; writing—original draft preparation, W.X.; writing—review and editing, W.X., Y.Z. (Yujun Zhang), K.I., H.W., Y.Z. (Yingcai Zhu), L.Z. and Z.G.; funding acquisition, W.X. All authors have read and agreed to the published version of the manuscript.

Institutional Review Board Statement: Not applicable.

Informed Consent Statement: Not applicable.

Data Availability Statement: Not applicable.

Conflicts of Interest: The authors declare no conflict of interest.

References

1. Polman, A.; Knight, M.; Garnett, E.C.; Ehrler, B.; Sinke, W.C. Photovoltaic materials: Present efficiencies and future challenges. *Science* **2016**, *352*, aad4424. [CrossRef]
2. Adachi, S. Optical Properties. In *Earth-Abundant Materials for Solar Cells*; John Wiley & Sons, Ltd.: Hoboken, NJ, USA, 2015; pp. 245–299.
3. Liu, M.-L.; Huang, F.-Q.; Chen, L.-D.; Chen, I.-W. A wide-band-gap *p*-type thermoelectric material based on quaternary chalcogenides of Cu2ZnSnQ4 (*Q* = S,Se). *Appl. Phys. Lett.* **2009**, *94*, 202103–202106. [CrossRef]
4. Shi, X.Y.; Huang, F.Q.; Liu, M.L.; Chen, L.D. Thermoelectric properties of tetrahedrally bonded wide-gap stannite compounds Cu2ZnSn1−xInxSe4. *Appl. Phys. Lett.* **2009**, *94*, 122103. [CrossRef]
5. Zhu, Y.; Liu, Y.; Ren, G.; Tan, X.; Yu, M.; Lin, Y.-H.; Nan, C.-W.; Marcelli, A.; Hu, T.; Xu, W. Lattice Dynamics and Thermal Conductivity in Cu2Zn1−xCoxSnSe4. *Inorg. Chem.* **2018**, *57*, 6051–6056. [CrossRef] [PubMed]
6. Huang, W.; Zhu, Y.; Liu, Y.; Liu, L.; Yang, C.; Xu, W. Unveiling the atomic defects and electronic structure of Cu2.2Zn0.8SnSe4−xTex (x = 0 to 0.04) by X-ray absorption fine structure spectroscopy. *Phys. Chem. Chem. Phys.* **2020**, *22*, 9362–9367. [CrossRef] [PubMed]
7. Chen, S.; Gong, X.G.; Walsh, A.; Wei, S.-H. Crystal and electronic band structure of Cu2ZnSnX4 (X=S and Se) photovoltaic absorbers: First-principles insights. *Appl. Phys. Lett.* **2009**, *94*, 041903–041905. [CrossRef]
8. Chen, S.; Walsh, A.; Gong, X.-G.; Wei, S.-H. Classification of Lattice Defects in the Kesterite Cu2ZnSnS4 and Cu2ZnSnSe4 Earth-Abundant Solar Cell Absorbers. *Adv. Mater.* **2013**, *25*, 1522–1539. [CrossRef]
9. Hall, S.R.; Szymanski, J.T.; Stewart, J.M. Kesterite, Cu<2) (Zn,Fe)SnS<4), and stannite, Cu<2) (Fe,Zn)SnS<4), structurally similar but distinct minerals. *Can. Mineral.* **1978**, *16*, 131–137.
10. Schorr, S. The crystal structure of kesterite type compounds: A neutron and X-ray diffraction study. *Sol. Energy Mater. Sol. Cells* **2011**, *95*, 1482–1488. [CrossRef]
11. Bosson, C.J.; Birch, M.T.; Halliday, D.P.; Knight, K.S.; Gibbs, A.S.; Hatton, P.D. Cation disorder and phase transitions in the structurally complex solar cell material Cu2ZnSnS4. *J. Mater. Chem. A* **2017**, *5*, 16672–16680. [CrossRef]
12. Stone, K.H.; Christensen, S.T.; Harvey, S.P.; Teeter, G.; Repins, I.L.; Toney, M.F. Quantifying point defects in Cu2ZnSn(S,Se)4 thin films using resonant x-ray diffraction. *Appl. Phys. Lett.* **2016**, *109*, 161901. [CrossRef]
13. Többens, D.M.; Gurieva, G.; Levcenko, S.; Unold, T.; Schorr, S. Temperature dependency of Cu/Zn ordering in CZTSe kesterites determined by anomalous diffraction. *Phys. Status Solidi* **2016**, *253*, 1890–1897. [CrossRef]
14. Schelhas, L.T.; Stone, K.H.; Harvey, S.P.; Zakhidov, D.; Salleo, A.; Teeter, G.; Repins, I.L.; Toney, M.F. Point defects in Cu2ZnSnSe4 (CZTSe): Resonant X-ray diffraction study of the low-temperature order/disorder transition. *Phys. Status Solidi* **2017**, *254*, 1700156. [CrossRef]
15. Többens, D.M.; Gurieva, G.; Niedenzu, S.; Schuck, G.; Zizak, I.; Schorr, S. Cation distribution in Cu2ZnSnSe4, Cu2FeSnS4 and Cu2ZnSiSe4 by multiple-edge anomalous diffraction. *Acta Crystallogr. Sect. B Struct. Sci. Cryst. Eng. Mater.* **2020**, *76*, 1027–1035. [CrossRef]
16. Bianconi, A.; Garcia, J.; Benfatto, M. XANES in condensed systems. In *Synchrotron Radiation in Chemistry and Biology I*; Springer: Berlin/Heidelberg, Germany, 1988; pp. 29–67.
17. Vergniory, M.G.; Wieder, B.J.; Elcoro, L.; Parkin, S.S.P.; Felser, C.; Bernevig, B.A.; Regnault, N. All topological bands of all nonmagnetic stoichiometric materials. *Science* **2022**, *376*, eabg9094. [CrossRef] [PubMed]
18. Călugăru, D.; Chew, A.; Elcoro, L.; Xu, Y.; Regnault, N.; Song, Z.-D.; Bernevig, B.A. General construction and topological classification of crystalline flat bands. *Nat. Phys.* **2022**, *18*, 185–189. [CrossRef]
19. Vergniory, M.G.; Elcoro, L.; Felser, C.; Regnault, N.; Bernevig, B.A.; Wang, Z. A complete catalogue of high-quality topological materials. *Nature* **2019**, *566*, 480–485. [CrossRef]
20. Bradlyn, B.; Elcoro, L.; Cano, J.; Vergniory, M.G.; Wang, Z.; Felser, C.; Aroyo, M.I.; Bernevig, B.A. Topological quantum chemistry. *Nature* **2017**, *547*, 298–305. [CrossRef]
21. Bunău, O.; Joly, Y. Full potential x-ray absorption calculations using time dependent density functional theory. *J. Phys. Condens. Matter* **2012**, *24*, 215502–215506. [CrossRef]
22. Huang, W.; Zhu, Y.; Liu, Y.; Tao, S.; Yang, C.; Diao, Q.; Hong, Z.; Han, H.; Liu, L.; Xu, W. Long-range ordering and local structural disordering of BiAgSe2 and BiAgSeTe thermoelectrics. *Phys. Chem. Chem. Phys.* **2021**, *23*, 24328–24335. [CrossRef]

23. Isotta, E.; Syafiq, U.; Ataollahi, N.; Chiappini, A.; Malerba, C.; Luong, S.; Trifiletti, V.; Fenwick, O.; Pugno, N.M.; Scardi, P. Thermoelectric properties of CZTS thin films: Effect of Cu–Zn disorder. *Phys. Chem. Chem. Phys.* **2021**, *23*, 13148–13158. [CrossRef] [PubMed]

24. Bourdais, S.; Choné, C.; Delatouche, B.; Jacob, A.; Larramona, G.; Moisan, C.; Lafond, A.; Donatini, F.; Rey, G.; Siebentritt, S.; et al. Is the Cu/Zn Disorder the Main Culprit for the Voltage Deficit in Kesterite Solar Cells? *Adv. Energy Mater.* **2016**, *6*, 1502276. [CrossRef]

25. Joly, Y. X-ray absorption near-edge structure calculations beyond the muffin-tin approximation. *Phys. Rev. B* **2001**, *63*, 125120. [CrossRef]